Available online at www.sciencedirect.com
SCIENCE DIRECT®
Journal of Power Sources 123 (2003) 151–162
JOURNAL OF POWER SOURCES
www.elsevier.com/locate/jpowsour

Carburisation of interconnect materials in solid oxide fuel cells

Li Jian [a], Jose Huezo [a], Douglas G. Ivey [b,*]

[a] *Global Thermoelectric Inc., Calgary, Alberta, Canada T2B 3R2*
[b] *Department of Chemical and Materials Engineering, University of Alberta, Edmonton, Alberta, Canada T6G 2G6*

Received 11 March 2003; accepted 30 March 2003

Abstract

Reformed fuel gases utilized in solid oxide fuel cells (SOFCs) contain significant amounts of carbon in the form of CO and CO_2. Alloys, such as ferritic stainless steels, which are utilized as interconnect materials in intermediate temperature SOFCs may, therefore, be susceptible to carburisation. Long-term exposure of ferritic stainless steel, with and without a nickel protective layer, to simulated carbon-containing fuel gas environments has been studied. Optical and electron microscopy (both SEM and TEM) techniques were utilized to characterize the microstructures prior to and after carburising.

Keywords: Solid oxide fuel cells; Interconnects; Carburisation; Electron microscopy

1. Introduction

Solid oxide fuel cells (SOFCs) are attractive for a number of energy related applications, including remote, automotive and residential power generation. Their use permits greater flexibility and cost savings as well as the potential for a reduction in harmful emissions. Fuel cells using yttria stabilized zirconia (YSZ) as the electrolyte operate at high temperatures (700–1000 °C), presenting a number of materials engineering challenges, related to the fabrication, operation and long-term reliability of the components [1–3]. One important component in a fuel cell system is the interconnect, which is utilized to electronically connect anodes and cathodes to one another when cells are stacked together in series. In addition to the obvious requirement of being electronically conductive, interconnect materials must have low ionic conductivity, have similar thermal expansion coefficients to other fuel cell components, be easy to fabricate, be stable at operating temperatures and act as a barrier to prevent mixing of fuel and oxidizing gases [3].

Candidate interconnect materials can be divided into two major types, electronically conductive oxides and oxidation resistant metallic alloys [3–5]. So-called high temperature solid oxide fuel cells (HTSOFCs) operate at 1000 °C and require the use of conductive oxides, such as $LaCrO_3$, as interconnects. Intermediate temperature solid oxide fuel cells (ITSOFCs) operate in the 700–750 °C range, making it feasible to use conventional oxidation resistant alloys, such as ferritic stainless steels, as interconnects. Ferritic stainless steels have many advantages relative to their ceramic counterparts, including good mechanical stability, high thermal and electronic conductivities, little porosity, ease of fabrication and significantly lower cost. A major concern, however, is the long-term reliability of ferritic stainless steels in fuel cell environments. Issues that need to be addressed include oxide scale growth, chromium vaporization and carburisation in reformed fuel gases present at the anode.

The goal of this work is to address the last issue, i.e. the potential for carburisation, as this can lead to carbide formation in the steel, resulting in embrittlement and loss of oxidation resistance (due to the consumption of Cr). Two kinds of samples are examined and compared, ferritic stainless steel and ferritic stainless steel with a protective Ni layer. Optical and electron microscopy techniques are utilized to examine the microstructure prior to and after exposure to the carburising environment.

2. Experimental methods

Two types of samples were exposed to carburising atmospheres. Both samples were ferritic stainless steels, nominally containing 16–18 wt.% Cr. One set of samples was cladded on both sides with Ni, in an attempt to provide oxi-

* Corresponding author. Tel.: +1-780-492-3321; fax: +1-780-492-2881.
E-mail address: doug.ivey@ualberta.ca (D.G. Ivey).

0378-7753/$ – see front matter © 2003 Elsevier Science B.V. All rights reserved.
doi:10.1016/S0378-7753(03)00535-4

dation protection, since Ni remains metallic in the anode gas atmosphere of the SOFC. The cladded samples were supplied by Technical Materials Inc. (TMI). The starting material for roll cladding was steel strip approximately 6–8 times the final thickness, with a proportionally suitable thickness of wrought pure Ni strip. The metal strips were mechanically and chemically cleaned, followed by cold bonding in a high pressure rolling mill with 70–75% reduction in a single pass. The metals extrude at different rates, but exited the rolls at the desired ratio of 1:8:1 (Ni:steel:Ni). The cladded steel was then annealed for a few seconds at 750 °C in a H_2 atmosphere to allow recrystallization to occur and diffusion bonding between the Ni and steel. The resultant composite was rolled to the final gauge thickness, annealed and sectioned. The final composite material consisted of a steel substrate ∼200 μm thick, with ∼25 μm of Ni of either side (total thickness of ∼250 μm). All samples were then annealed at 750 °C for up to 1000 h in a simulated reformed fuel environment—53.09% N_2, 25.19% H_2, 18.26% CO, 3.27% CO_2 and 0.17% CH_4.

Cross-section samples for optical microscopy and SEM analysis were prepared using standard metallographic techniques. After mounting and polishing, samples were etched with Vilella's reagent (1 g picric acid, 5 ml HCl, 100 ml ethanol) [6]. Vilella's reagent is good for bringing out second phase particles and the ferrite grain structure. Samples were examined in either a LEO 1450VP (variable pressure) SEM or a Hitachi H2700 SEM, both equipped with ultra-thin window (UTW) X-ray detectors.

Two types of TEM specimens were prepared, i.e. carbon extraction replicas and thin foils. Replicas were primarily utilized to isolate and characterize carbides, while foils were used for overall microstructure examination and matrix phase identification. Thin foils were prepared as cross sections, through a combination of mechanical polishing and ion milling, to allow characterization of microstructure as a function of depth from the surface. Replicas and foils were examined in either a JEOL 2010 TEM or a Technai F20 field emission gun (FEG) TEM/STEM, both equipped with UTW X-ray detectors.

Table 1
Carbon analysis (wt.%) for tested steels

Sample	As received	350 h	700 h	1000 h
Ferritic steel	0.051	0.050	0.052	0.048
Ni-clad ferritic steel	0.043	0.210	0.220	0.240

3. Results and discussion

The carbon content in the steel samples, both in the as received condition and after annealing, is shown in Table 1. The as received compositions for the two samples are similar—∼0.05 wt.%. The Ni-clad sample has 15–20% less carbon, because the Ni layers were included in the analysis. After exposure to the simulated reformed fuel, the carbon content in the ferritic steels does not change, even after exposure for 1000 h. The carbon content in the Ni-clad steels increases almost six-fold after exposure for 350 h followed by a slight increase with increasing exposure. The reasons for the differences will be discussed in the following sections.

An optical micrograph of the as received ferritic stainless steel is shown in Fig. 1. The microstructure is typical of

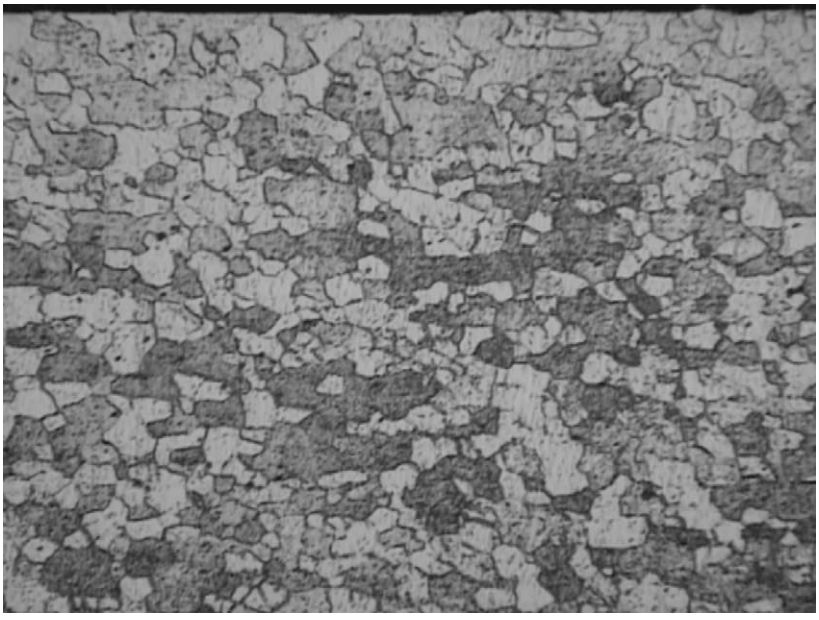

Fig. 1. Optical micrograph of as received ferritic stainless steel, showing ferrite grains and dispersion of Cr-rich carbides.

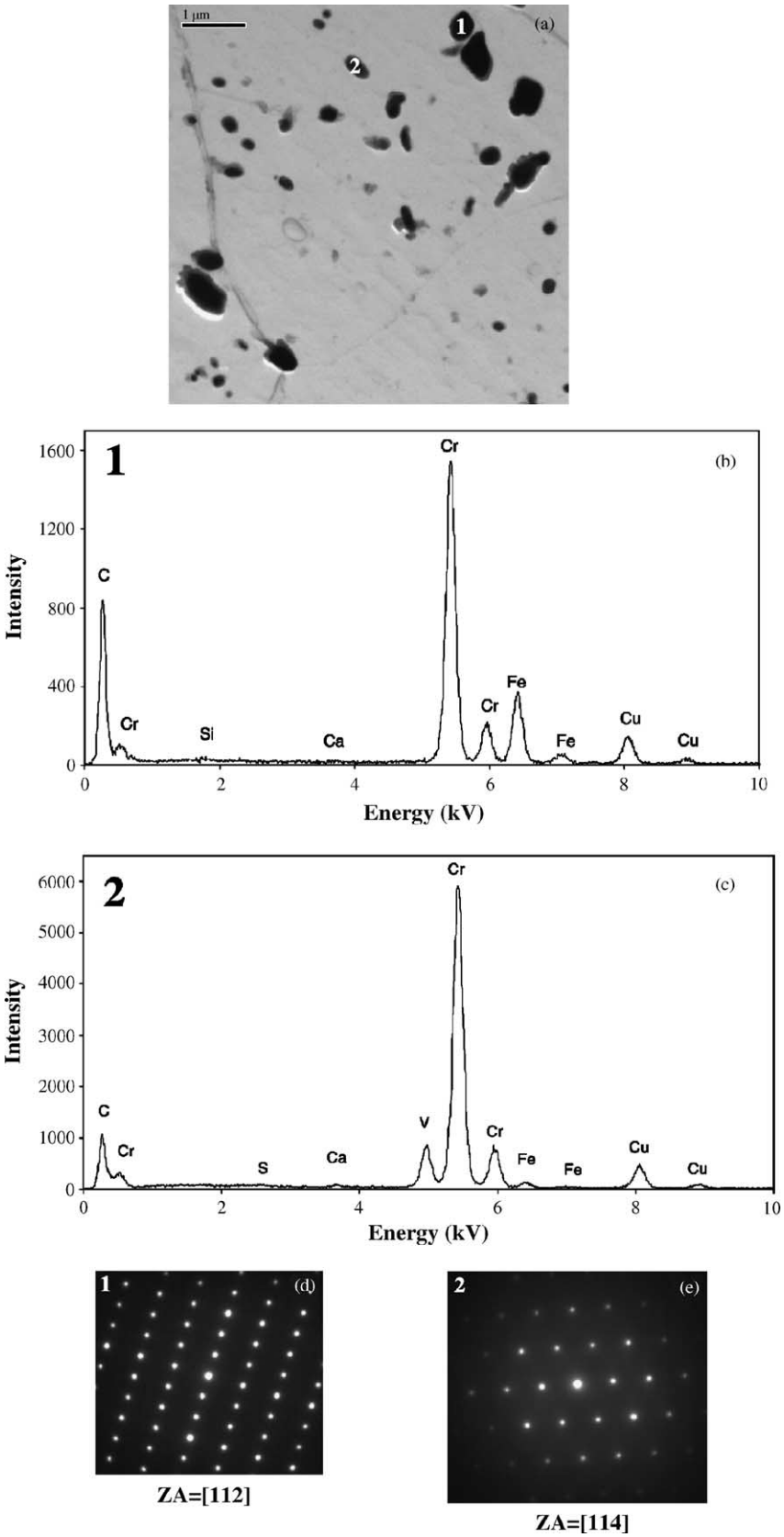

Fig. 2. (a) TEM BF micrograph of carbon extraction replica from as received ferritic stainless steel, showing carbides; (b) and (c) EDX spectra from particles indicated in (a); (d) and (e) SAD patterns from particles indicated in (a). Zone axes are indicated based on $M_{23}C_6$ designation.

this type of steel, consisting of a ferritic matrix and Cr-rich carbides [6,7]. Extraction replicas were examined to identify the carbides through electron diffraction and energy dispersive X-ray (EDX) analysis in the TEM. A representative bright field (BF) micrograph, as well as selected area diffraction (SAD) patterns and EDX spectra are shown in Fig. 2. Carbides are present both within the ferrite grains and at the grain boundaries. Based on EDX analysis, two types of Cr-rich carbides were identified—those containing Fe and V and those with Fe only. It is interesting to note that V is not normally specified as an alloying element in ferritic grades of stainless steels, but is clearly present in this steel likely as an impurity. No V was detected in the ferrite matrix; vanadium's presence in the carbides can be attributed to its high affinity for carbon. Both carbides had the same crystal structure and were indexed as $M_{23}C_6$ (M: Cr, Fe, V, or M: Cr, Fe), which is cubic with $a = 1.066$ nm. This carbide is expected for ferritic stainless steels containing <18 wt.% Cr [6,7].

Optical micrographs of the unclad stainless steel, exposed to the carburising environment for 350 and 1000 h, are shown in Fig. 3. The microstructures, in both cases, are very similar to the as received sample (Fig. 2), with the exception of a thicker surface (Cr/Fe-rich) oxide layer. The oxide layer is easier to discern in the SEM secondary electron (SE) image in Fig. 4. The carbides are similar in size, composition and

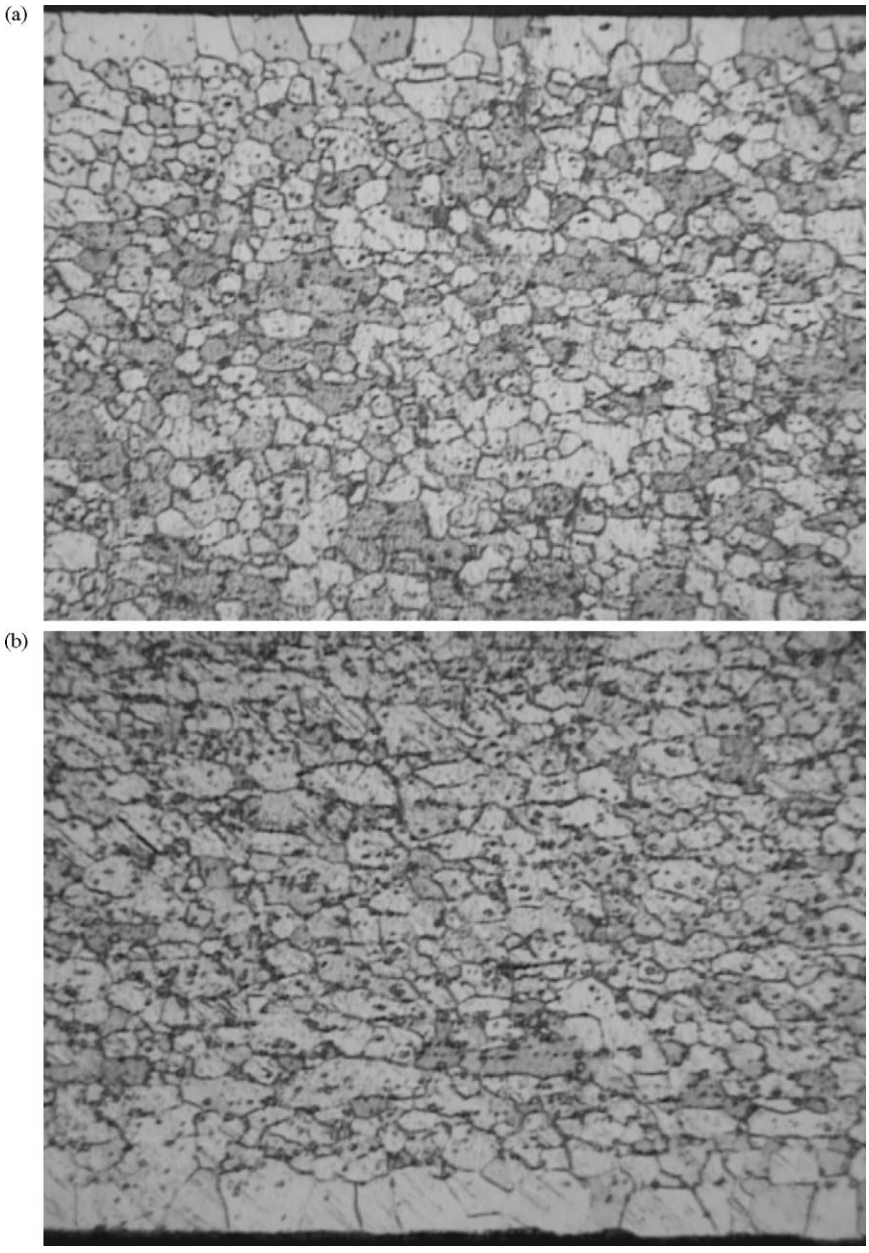

Fig. 3. Optical micrographs of ferritic stainless steel, exposed to simulated fuel at 750 °C for: (a) 350 h and (b) 1000 h.

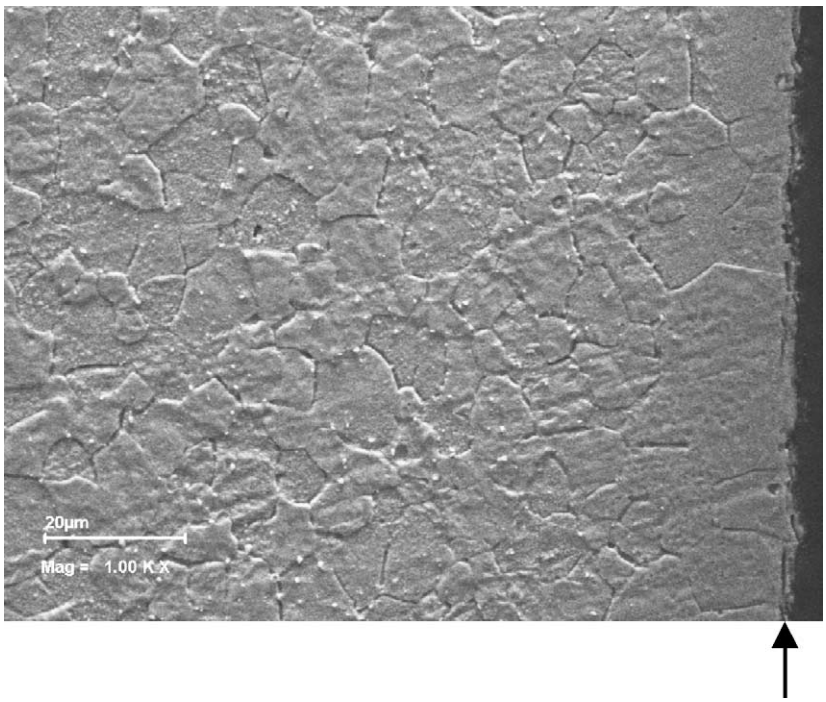

Fig. 4. SEM SE image of ferritic stainless steel, exposed to simulated fuel at 750 °C for 350 h. The oxide layer on the surface is indicated by the arrow.

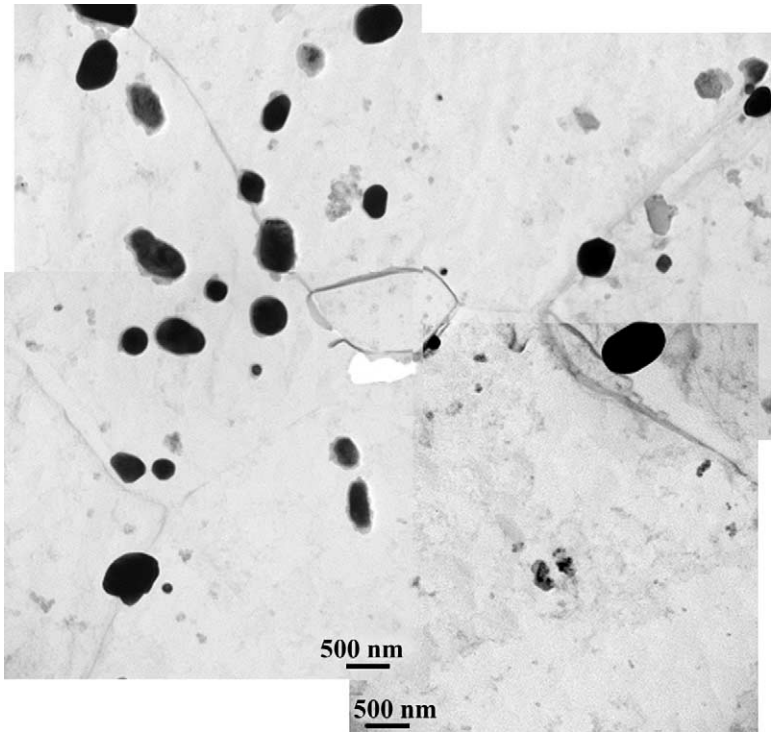

Fig. 5. TEM BF image of carbon extraction replica from ferritic stainless steel, exposed to simulated fuel at 750 °C for 1000 h.

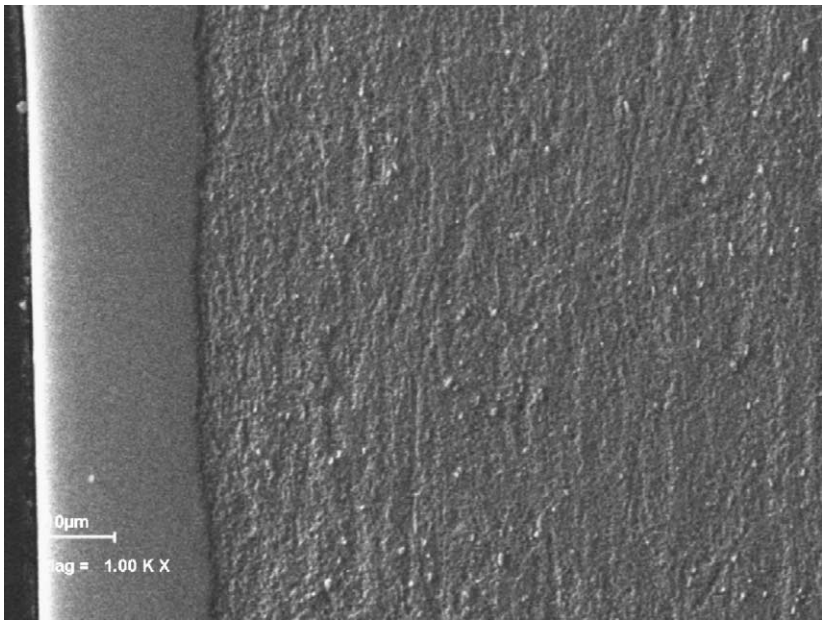

Fig. 6. SEM SE image of as clad (Ni) stainless steel.

morphology (Fig. 5) to those in the as received sample. The oxide layer that forms on the surface of the steel appears to act as a barrier to carbon diffusion into the surface, which is driven by the higher carbon activity in the atmosphere relative to the steel.

An SE image of the Ni-clad steel, in the as-clad condition, is shown in Fig. 6. The Ni cladding is clearly visible and the steel microstructure is very similar to the unclad material. The Cr-rich carbides are clearly visible; however, the ferrite grain boundaries are not clearly delineated. Good quality metallographic specimens were difficult to prepare because of significant hardness differences between the Ni and stainless steel.

Optical micrographs and SEM SE images from the Ni-clad steel, exposed to the carburising environment for 350 and 1000 h, are shown in Figs. 7 and 8. Significant microstructural changes have occurred. Large precipitates (>2 μm) have formed at the ferrite grain boundaries in the matrix. These are Cr-rich (Fig. 9a) and are likely carbides. In addition, there is an apparent increase in the cladding thickness, from 25 μm in the as clad condition to ∼40 μm after 350 h to ∼60 μm after 1000 h. This is a result of Fe and Ni interdiffusion producing an alloyed layer at the surface. The composition of the alloyed layer is variable, ranging from Ni-rich at the surface to Fe-rich in the interior (Fig. 9b and c). Cracks are also present throughout this alloyed layer and become more pronounced for longer exposure times. The regions within the cracks are oxidized, comprising primarily Cr oxide with smaller amounts of Fe and Ni oxide (Fig. 9d).

Extraction replicas produced from the Ni-clad steel, after long-term exposure to the simulated fuel, did not retain any of the large precipitates (>2 μm) as evident in Fig. 10. These particles were too large to be lifted out. As such, cross-section thin foils were prepared of these samples. A representative STEM image, with large carbides at the ferrite grain boundaries, is shown in Fig. 11a. The image is an annular dark field (DF) image, which has been inverted to resemble a conventional TEM BF image. An X-ray linescan, across one of the particles and the adjacent ferrite matrix, shows that the particle is a Cr–Fe carbide (Fig. 11b and c). Note that the carbon linescan has been re-plotted in Fig. 11c, with the vertical scale expanded, to emphasize the C distribution. No V was detected in any of the large carbides, as all available V was consumed in carbide formation in the as received steel. SAD patterns were obtained from the large carbides and were indexed as $M_{23}C_6$ (M: Cr, Fe). A representative pattern is shown in Fig. 11d.

A STEM image (inverted annular DF image) of the near surface region of the Ni-clad sample, exposed to the simulated fuel for 1000 h, is shown in Fig. 12a. The area shown consists of several grains, composed of primarily Fe and Ni with smaller amounts of Cr and Si (Fig. 12b), as well as cracks running along the grain boundaries. The cracks correspond to those observed in the SEM (see Fig. 8) and are oxidized along their surfaces (Fig. 12c). The oxide is Cr-rich (likely Cr_2O_3), but contains small amounts of Fe and Ni. There may be some Si in the mixed oxides; however, not likely to the level shown in the EDX spectrum. Most of the Si is an artifact of the TEM sample preparation process, i.e. it is present in the epoxy used to glue pieces together to form cross sections. The Si present in the Fe–Ni grains is not an artifact, as ferritic stainless steels contain ∼1.0 wt.% Si. Several SAD patterns were obtained from the Fe–Ni phase—a representative pattern is shown in Fig. 12d.

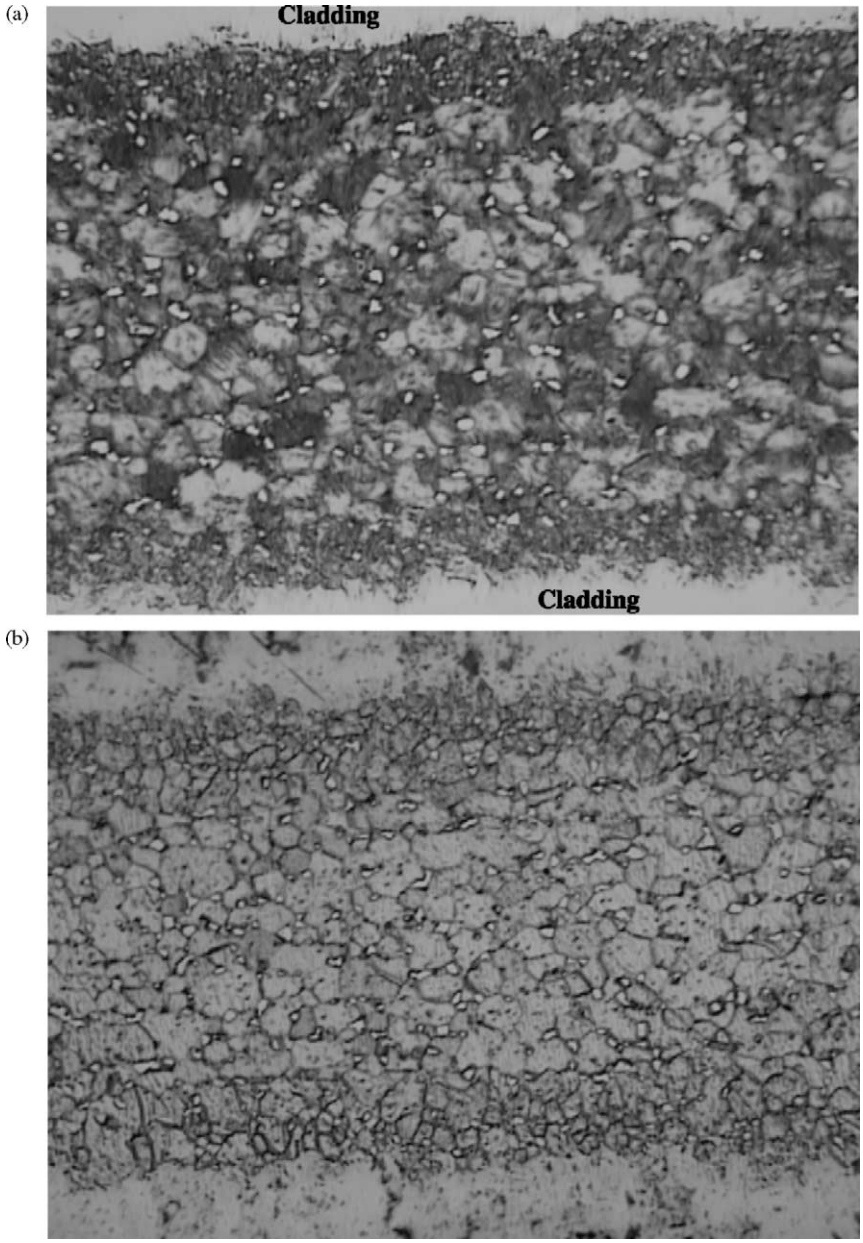

Fig. 7. Optical micrographs of Ni-clad ferritic stainless steel, exposed to simulated fuel at 750 °C for: (a) 350 h and (b) 1000 h. Note the presence of large particles at the ferrite grain boundaries.

The patterns could be indexed to either $FeNi_3$ or γ(Fe, Ni), a fcc solid solution phase of Fe and Ni. Both the phases have similar crystal structures (cubic) and lattice parameters ($a = 0.350$–0.360 nm). The γ phase was chosen as the better fit for two reasons. $FeNi_3$ is only stable below 517 °C [8] and, therefore, would not have formed during testing at 750 °C. It is unlikely that transformation to ordered $FeNi_3$ would have occurred during cooling to room temperature, because of kinetic limitations. Also, the composition range for $FeNi_3$ is ∼64–90 wt.% Ni, while the γ phase exists over almost the entire composition range (from ∼10 to 100 wt.% Ni at 750 °C). As evident from the EDX spectra in Fig. 9, the composition of the alloyed layer is quite variable. γ(Fe, Ni) can also dissolve in excess of 35 wt.% Cr at 750 °C [8], which would account for the significant amount of Cr present.

Based on the above results, there is clearly no benefit to Ni cladding the surface of the ferritic stainless steel. In fact, the Ni cladding is detrimental, enhancing carbon diffusion into the bulk steel and Cr diffusion out of the steel. Chromium must diffuse to the surface primarily by a grain boundary mechanism, initially through the Ni and then later through the γ(Fe, Ni) phase, since a uniform Cr oxide is not formed on the surface. Further evidence that grain boundary diffusion predominates can be gleaned from estimated bulk diffusion distances for Cr in Ni. These

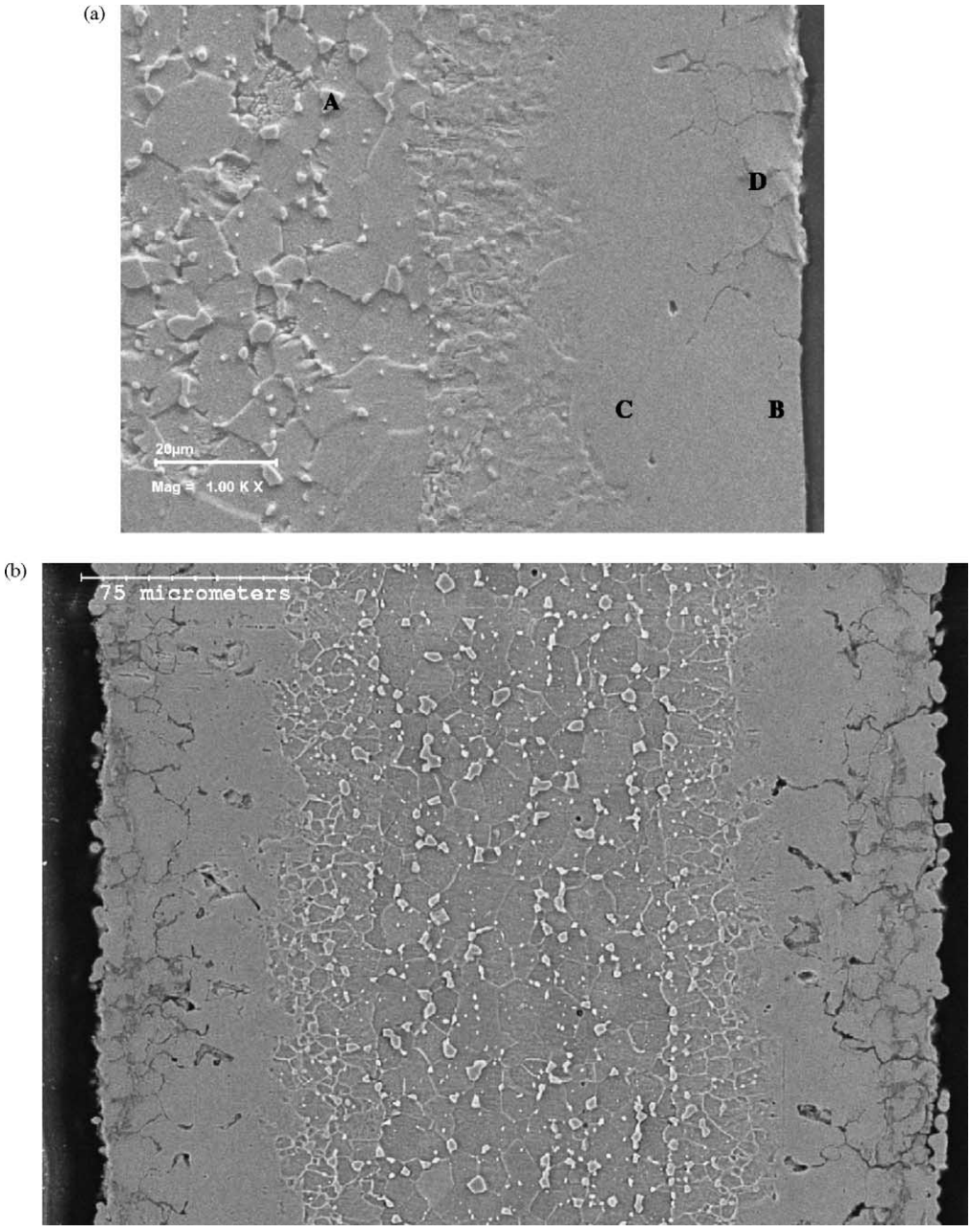

Fig. 8. SEM SE images of Ni-clad ferritic stainless, exposed to simulated fuel at 750 °C for: (a) 350 h and (b) 1000 h.

are <4 μm for 1000 h exposure [9], which is significantly less than the cladding thickness. The oxide formed is localized to the grain boundaries, causing crack formation along the boundaries emanating from the surface and moving inwards. The cracking actually enhances the carburisation process. Oxidation is driven thermodynamically by the lower free energy for Cr_2O_3 formation relative to CO or CO_2. The standard free energies of formation for Cr_2O_3, CO and CO_2 at 750 °C are approximately −570, −410 and −400 kJ/mol (of O_2), respectively, [10]. For long-term operation, grain boundary oxidation of the Ni (or γ(Fe, Ni)) layer will dramatically increase the electrical resistance of the interconnect, if each grain is surrounded by oxide.

Carburisation of the steel has two negative consequences. Chromium is consumed in carbide formation, reducing the amount available for corrosion or oxidation protection and the formation of large carbides along the ferrite grain boundaries can embrittle the steel. Calculations, based on some simplifying assumptions, can be done to estimate the amount of Cr consumed in carbide formation.

After carburising for 1000 h at 750 °C, the Ni-clad steel contained about 5.6 times the amount of carbon relative to the as received steel. The measured carbon levels were

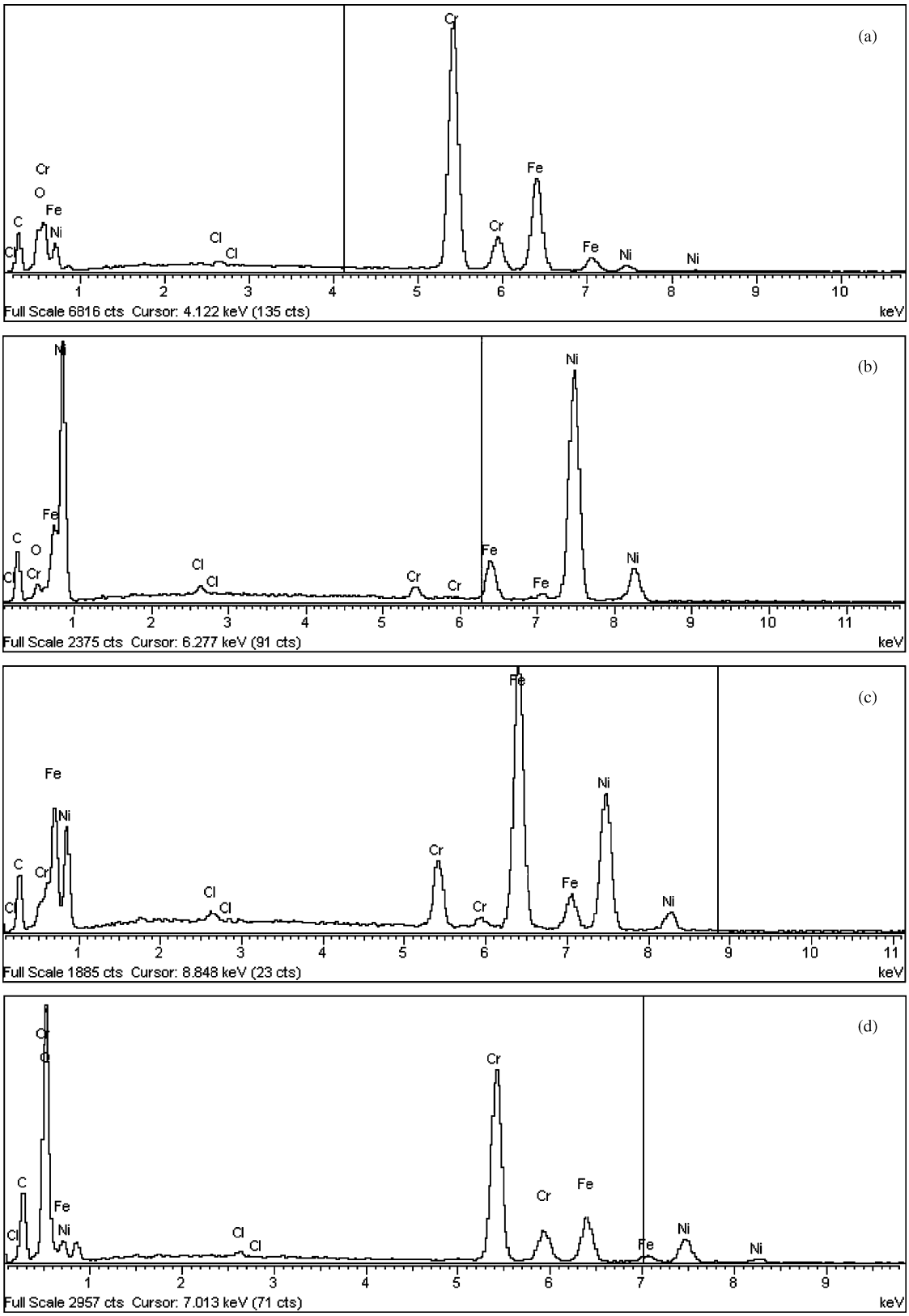

Fig. 9. EDX spectra taken from the regions indicated in Fig. 8a. EDX spectrum from: (a) large carbide particle; (b) alloyed cladding layer near the surface; (c) alloyed cladding layer near interface with steel; (d) within a crack in alloyed cladding layer.

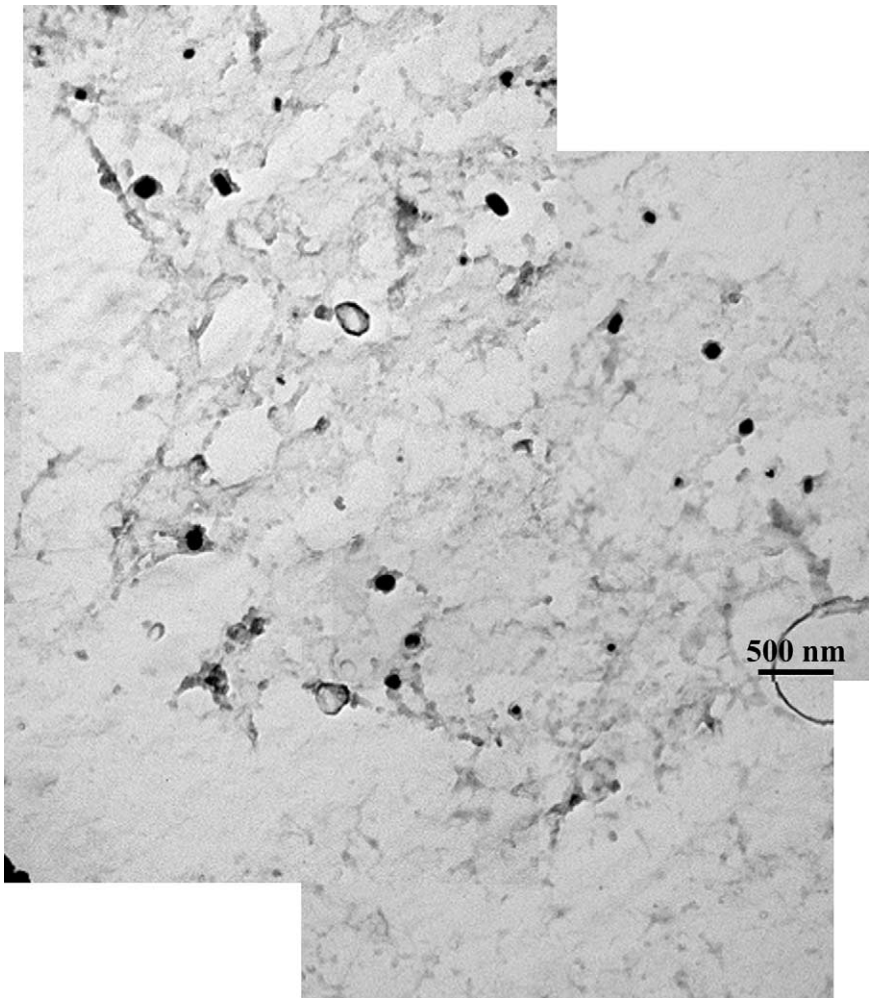

Fig. 10. TEM BF image of carbon extraction replica from Ni-clad ferritic stainless steel, exposed to simulated fuel at 750 °C for 1000 h.

0.043 and 0.240 wt.%, respectively, for the as received and carburised conditions. The actual carbon levels in the steel itself were likely higher in both cases, when the Ni layers are accounted for. No carbon was present in the Ni layer of the as received sample or in the alloyed γ(Fe, Ni) layer after carburising. The carbon level in the as clad steel is, therefore, closer to the 0.05 wt.% value measured for the unclad as received steel. The actual amount of carbon in the carburised steel is more difficult to estimate because of the variable composition of the alloyed Ni–Fe layer, but a ballpark figure can be calculated based on the following analysis. The average composition of the γ phase is assumed to be 50% Ni (either wt.% or at.% is suitable as Ni and Fe have very similar atomic weights), and the densities of Ni, α-Fe and γ(Fe, Ni) are 8.9, 7.86 and 8.0 g/cm^3, respectively. If all the Ni cladding (∼50 μm) is consumed, then ∼57 μm of the steel will be consumed in forming γ(Fe, Ni), leaving 143 μm of unreacted steel. This will result in the formation of ∼110 μm of γ(Fe, Ni), or 55 μm on each side. The thicknesses correspond reasonably well to those measured from Fig. 8b (1000 h at 750 °C). The unreacted steel is ∼150 μm thick, while the alloyed surface layer is ∼60 μm thick on each side. Based of these simple calculations, the carbon content in the steel itself is ∼33% higher than the measured value in Table 1, giving a carbon level of ∼0.32 wt.%. Since the solubility of carbon in ferrite is quite low (∼0.022 wt.% at 727 °C and ∼0.008 wt.% at room temperature), virtually all the carbon must be contained in carbides. The amount of Cr consumed can, therefore, be estimated, after making some simplifying assumptions. The Cr level in the steel is taken as 16 wt.% (lower end of the specifications) and the carbide chemistry is taken as $Cr_{23}C_6$. The relatively small amounts of Fe and V are ignored for simplicity. The amount of Cr, which has diffused towards the surface forming oxide within the surface cracks, has also been ignored which should somewhat offset the errors in omitting Fe and V in the carbide. There is Cr present in the γ(Fe, Ni) phase, at relative Cr/Fe levels similar to those in the ferrite matrix. Using the carbon level of 0.32 wt.% estimated above, approximately one-third of the Cr in the steel would be consumed in forming $Cr_{23}C_6$, leaving the Cr level in the steel at ∼10.5–11 wt.% Cr. As mentioned above,

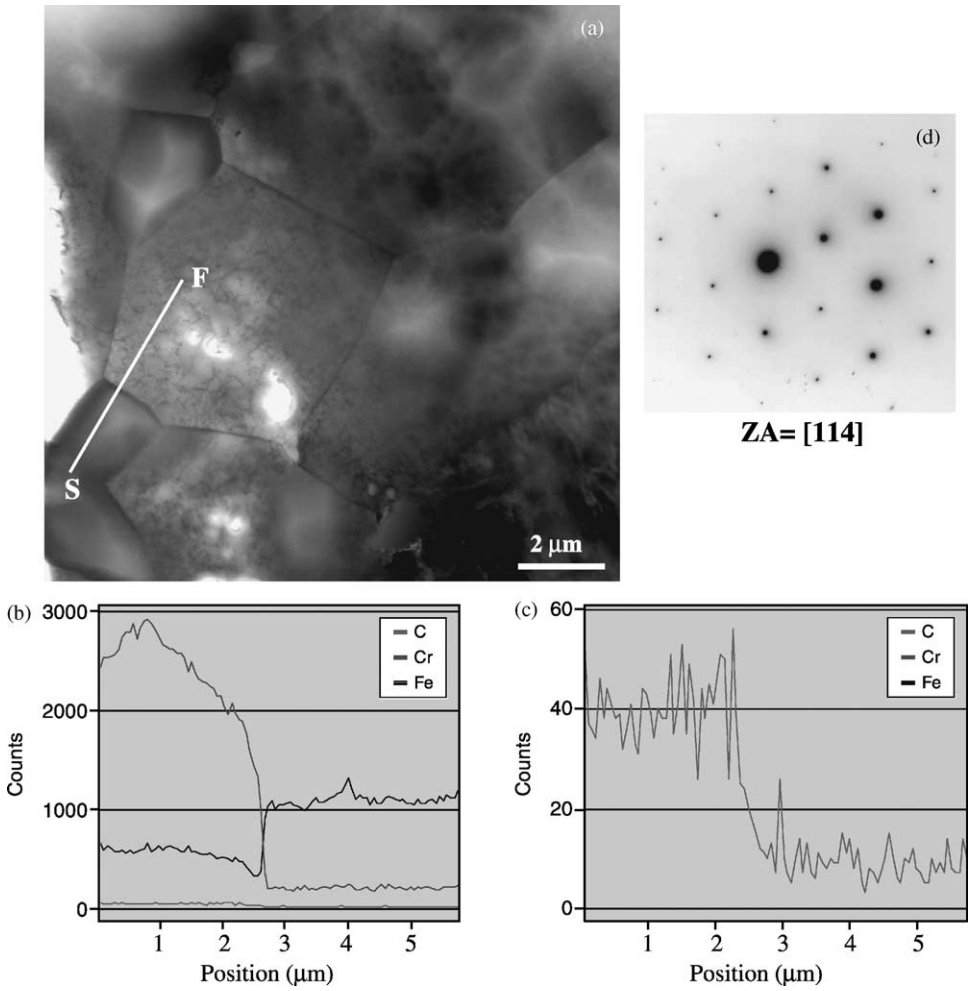

Fig. 11. (a) STEM image of thin foil sample, prepared from Ni-clad ferritic stainless steel exposed to simulated fuel at 750 °C for 1000 h, showing large carbides in a ferrite matrix; (b) and (c) X-ray linescans across carbide particle and ferrite matrix; (d) SAD pattern from carbide particle in (a)—indexed as $M_{23}C_6$.

these calculations only provide estimates of C levels and Cr consumption.

The ferritic stainless steel, without any Ni cladding, is actually quite resistant to carburising at the test temperature examined. This result is counterintuitive, based on expected diffusion behavior. The diffusion coefficient for carbon diffusing interstitially in ferrite at 750 °C is $\sim 5 \times 10^{-7}$ cm^2/s [11], which translates to a diffusion distance (based on $x \approx (Dt)^{0.5}$) of ~8 mm for 350 h. This value far exceeds the 200 μm thickness of the steel. One would, therefore, expect the steel to be fully carburised, when, in fact, carbon levels do not change. This can be attributed to the Cr oxide that forms on the surface during exposure (Fig. 4) and acts as an effective carbon diffusion barrier.

4. Summary

The effect of a simulated fuel environment on the carburisation of ferritic stainless steels, used as an interconnect material in ITSOFCs, has been studied. Two types of steel samples were investigated, one with and one without a Ni cladding. The results are summarized as follows:

1. The unclad steel was resistant to carburisation, showing no discernible carbon pick-up even after exposure to the fuel for up to 1000 h at 750 °C. A chromium oxide layer, formed on the surface, acted as an effective diffusion barrier.
2. The Ni clad steel carburised readily in the fuel environment, with the steel showing an almost six-fold increase in carbon levels after exposure to the fuel for 1000 h.
3. Large (>2 μm) $M_{23}C_6$ (M: Cr, Fe) particles formed along ferrite grain boundaries, significantly reducing the Cr in solution in the ferrite.
4. The Ni cladding reacted with the Fe in the steel to form an alloyed γ(Fe, Ni) solid solution phase. This phase had numerous cracks with oxidized surfaces—primarily Cr_2O_3.

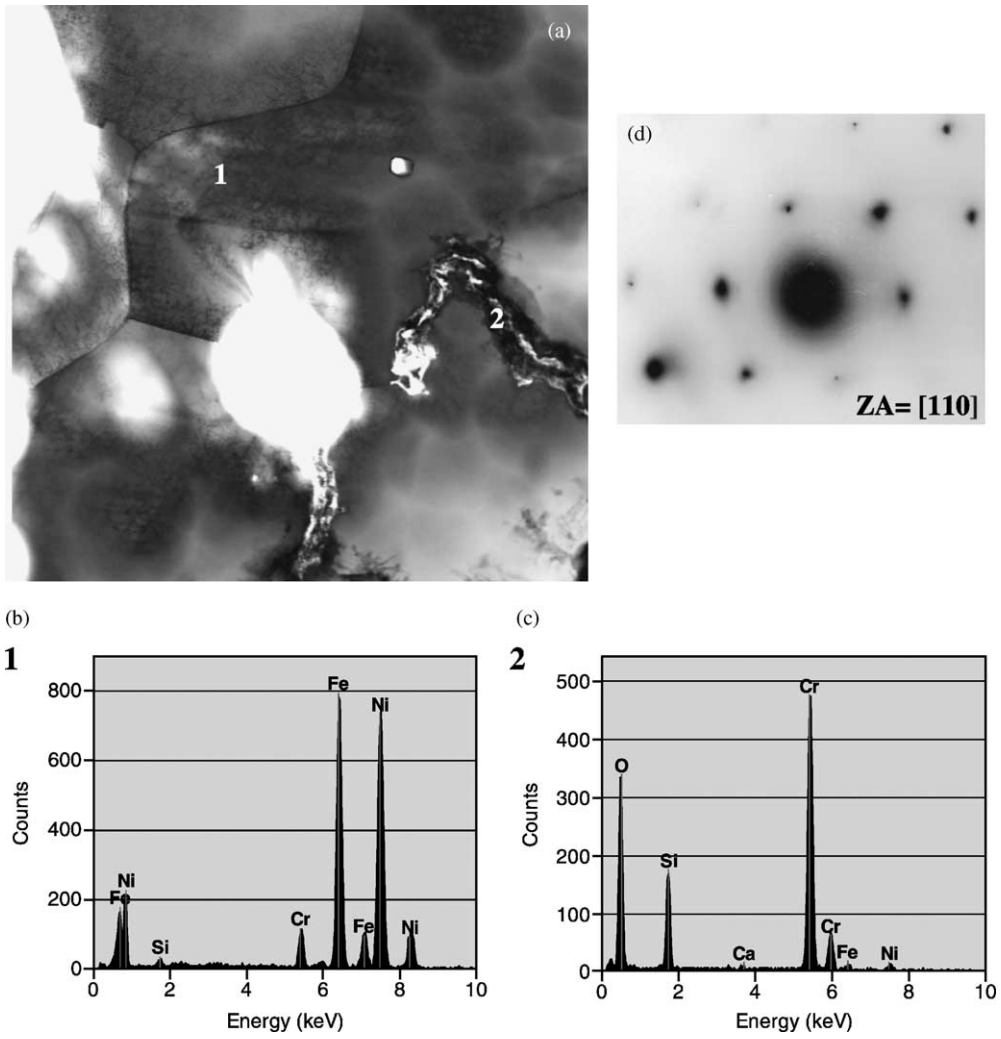

Fig. 12. (a) STEM image of thin foil sample, prepared from Ni-clad ferritic stainless steel exposed to simulated fuel at 750 °C for 1000 h, showing the alloyed Ni–Fe surface region; (b) EDX spectrum from grain indicated in (a); (c) EDX spectrum from oxide indicated in (a); (d) SAD pattern from grain indicated in (a). The pattern has been indexed as γ(Fe, Ni) with a zone axis near [1 1 0].

Acknowledgements

The authors would like to acknowledge the assistance of Ms. Julia Protkova and Dr. Anqiang He for assistance with the SEM analysis and Dr. Jijun Xu for providing the testing gas composition.

References

[1] B.C.H. Steele, J. Mater. Sci. 36 (2001) 1053.
[2] L. Carrette, K.A. Friedrich, U. Stimming, Fuel Cells 1 (2001) 5.
[3] H. Yokokawa, N. Sakai, T. Horita, K. Yamaji, Fuel Cells 1 (2001) 117.
[4] J.M. Ralph, A.C. Schoeler, M. Krumpelt, J. Mater. Sci. 36 (2001) 1161.
[5] S.P.S. Badwal, Solid State Ion. 143 (2001) 39.
[6] Metallography and microstructures, ASM Metals Handbook, Ninth ed., vol. 9, ASM, Metals Park, Ohio, 1985, pp. 279–286.
[7] W.F. Smith, Structure and Properties of Engineering Alloys, McGraw-Hill, New York, 1981, pp. 270–281.
[8] Alloy phase diagrams, ASM Handbook, vol. 3, ASM International, Metals Park, Ohio, 1992, pp. 2–199.
[9] C.J. Smithells, Metals Reference Book, Fourth ed., vol. II, Butterworths, London, 1967, pp. 664.
[10] D.R. Gaskel, Introduction to Thermodynamics of Materials, Third ed., Taylor and Francis, Washington, DC, 1995.
[11] R.J. Borg, G.H. Dienes, An Introduction to Solid State Diffusion, Academic Press Inc., San Diego, CA, 1988, pp. 60, 92.